NANO LETTERS

Letter

pubs.acs.org/NanoLett

Lattice Relaxation at the Interface of Two-Dimensional Crystals: Graphene and Hexagonal Boron-Nitride

Jiong Lu,[†,‡,#] Lídia C. Gomes,[‡,§,#] Ricardo W. Nunes,[§] A. H. Castro Neto,[‡,∥] and Kian Ping Loh*[,†,‡]

[†]Department of Chemistry, National University of Singapore, 3 Science Drive 3, 117543, Singapore

[‡]Graphene Research Centre, National University of Singapore, 6 Science Drive 2, 117546, Singapore

[§]Departamento de Física, ICEx, Universidade Federal de Minas Gerais, Avenida Antônio Carlos 6627, Pampulha, 30123-970, Belo Horizonte, Minas Gerais, Brazil

[∥]Department of Physics, National University of Singapore, 2 Science Drive 3, 117542, Singapore

Supporting Information

ABSTRACT: Heteroepitaxy of two-dimensional (2D) crystals, such as hexagonal boron nitride (BN) on graphene (G), can occur at the edge of an existing heterointerface. Understanding strain relaxation at such 2D laterally fused interface is useful in fabricating hetero-interfaces with a high degree of atomic coherency and structural stability. We use in situ scanning tunneling microscopy to study the 2D heteroepitaxy of BN on graphene edges on a Ru(0001) surface with the aim of understanding the propagation of interfacial strain. We found that defect-free, pseudomorphic growth of BN on a graphene edge "substrate" occurs only for a short distance (<1.29 nm) perpendicular to the interface, beyond which misfit zero-dimensional dislocations occur to reduce the elastic strain energy. Boundary states originating from a coherent zigzag-linked G/BN boundary are observed to greatly enhance the local conductivity, thus affording a new avenue to construct one-dimensional transport channels in G/BN hybrid interface.

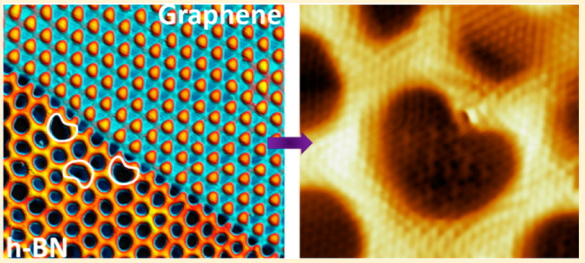

KEYWORDS: *Graphene, hexagonal boron nitride, hybrid film, lattice relaxation, misfit dislocations, interface electronic structures*

Heteroepitaxy of three-dimensional (3D) layered semiconducting heterojunctions has been an active area of research for many decades because of its technological relevance to solid state devices and circuits.[1,2] Heteroepitaxial growth of 2D lateral heterostructures, such as layered graphene and hexagonal boron nitride (G/BN) hybrids, has recently attracted attention because of the possibility to generate mixed alloyed phases with tunable electronic properties and also applications in lateral tunneling devices and plasmonics.[3−11] Such in-plane G/BN hybrid film with well-defined heterointerfaces has been theoretically predicted to possess novel magnetic and unique thermal transport properties.[12−16] Ci et al. demonstrated that a hybrid film with a tunable bandgap can be achieved on Cu foil by simultaneously supplying carbon and BN growth precursors. In such a one-step growth, the phase-separation leads to randomly mixed graphene and BN domains.[4] Patterned sequential growth has also been used for the spatially controlled growth of lateral junctions between graphene and BN to make integrated circuitry or close-loop resonators.[6,7] The possibility of forming an abrupt heterojunction between BN and G has stimulated a lot of interest owing to the prediction of an abundance of fascinating properties at such 1D interface.[17,18] Using different microscopy techniques, the successful interfacing of graphene and BN domains has been demonstrated on different metal surfaces, such as Ru(0001),[19] Rh(111),[17] and Cu(100).[5] There is great excitement regarding the observation of short-segments of sharp G/BN interface preferentially linked in the zigzag fashion.

However, many issues surrounding the formation of continuous and atomically sharp G/BN heterointerfaces remain unclear. Fault lines and cracks in hybrid films are mainly governed by interfacial strain.[20,21] However, there is no insight into how strain propagates along the length of such an interface and how the interfacial lattice relaxes to avoid the discontinuity of heterointerfaces. In addition, the electronic states are coupled to the underlying metal. Electronic decoupling of the G/BN interface from the metallic substrate is needed to reveal the intrinsic physical and electronic properties at the G/BN boundaries. To this end, we carried out STM studies to understand the strain relief mechanism at atomically abrupt G/BN interface as well as to probe the interfacial electronic states on the decoupled G/BN interface.

Results and Discussion. To synthesize hybrid thin films, a common strategy is based on the two-step sequential chemical vapor deposition (CVD). For in-plane G/BN heterostructures, the synthesis process usually involves a first stage growth of graphene (BN) islands or prepatterning of the graphene (BN) strips followed by a regrowth of BN (G) to cover the exposed

Received: May 21, 2014
Revised: July 22, 2014
Published: August 1, 2014

   dx.doi.org/10.1021/nl501900x | *Nano Lett.* 2014, 14, 5133−5139

metal surface. The edges of graphene (BN) serve as nucleation sites to seed the growth of BN (G). Owing to the lattice mismatch between graphene and BN, the edge-templated heterogrowth in 2D resembles mismatched heteroepitaxy of a thin film on a substrate. It is well-known that at the initial stage of 3D heteroepitaxy, such as the growth of a GaAs epilayer on a Si substrate, it is energetically favorable for the film embryo to be coherent with the substrate lattice (termed as pseudomorphic growth), in which the lattice mismatch is accommodated by elastic deformation of the epilayer.[22,23] The interfacial strain energy gradually builds up with the increase of film thickness. At a critical thickness, it becomes energetically favorable to relieve the strain by having a network of misfit dislocations at the interface, beyond which the epitaxial film is apt to return to its stable unstrained bulk structure (Figure 3a).[1,22] Misfit dislocations introduced in the epitaxy of 3D heterostructures generally pile up at the interfaces, which in turn degrades the atomic coherency and abruptness of fused heterointerfaces.[24] With the advent of the field of 2D materials, it is important to ask whether the 3D interfacial strain relaxation scenario also applies in 2D mismatched heteroepitaxy, and the length scale at which a defect-free G/BN heterointerface can be formed before dislocation or other defects set in to relieve the strain energy.

In order to study the heterogrowth behavior of in-plane G/BN heterojunctions, BN was grown on existing graphene patches on Ru(0001) surface. The BN and G domains can be easily distinguished by STM imaging due to the presence of characteristic Moiré blistering of graphene and "nanomesh" patterns of BN.[25−28] To make a sharp G/BN interface, the growth temperature and partial pressure of precursors were lowered. The growth temperature is reduced to suppress interfacial mixing resulting from metal-catalyzed atomic substitution at high temperature (>900 K). A low partial pressure (1×10^{-8} mbar) of hydrocarbon precursor is used to grow graphene islands to reduce the nucleation of graphene on the free Ru surface. Carbon adatoms attach to existing islands owing to its higher diffusivity coefficient at low flux conditions.[29−32] By sequentially exposing as-prepared clean Ru to C_2H_4 (5 Langmuirs (L)) and borazine (30 L) at 800 K (Figure 1a), we observe the pseudomorphic growth of BN strips on the edge of graphene. Short segments of an atomically sharp G/BN interface readily appears at the condition ($\mu_c/\mu_{B/N} < \sim 0.2$), where nanoscale graphene islands are surrounded by BN strips (Figure 1b). The majority of G/BN boundaries generated in this condition are atomically abrupt and their lengths lie in the range of 10 nm < L < 24 nm (Figure 1a,b). The seamless bonding between graphene and BN at the interface is revealed in the magnified STM image where the graphene Moiré hump (bright regions) always faces the nanomesh "pores" (dark regions) at the boundaries (Figure 1c). As resolved by high-resolution STM imaging (Figure 1d), graphene and BN connect in a zigzag fashion, which is in line with the previous report.[17]

An extended G/BN interface can be grown by increasing the coverage of preexisting graphene islands to 0.5 ML and subsequently filling the entire Ru gap region by the regrowth of BN (20 L; at low partial pressure, 10−8 mbar). The resulting 1D G/BN interface has a length scale of 100−200 nm (Figure 2a). Interestingly, we observed three types of irregularities in BN domains embedded in the matrix of graphene islands at this growth condition, including random moiré patterns formed at some distances away from the G/BN interface, discontinuities (indicated by the missing BN moiré wires) and heart-shaped

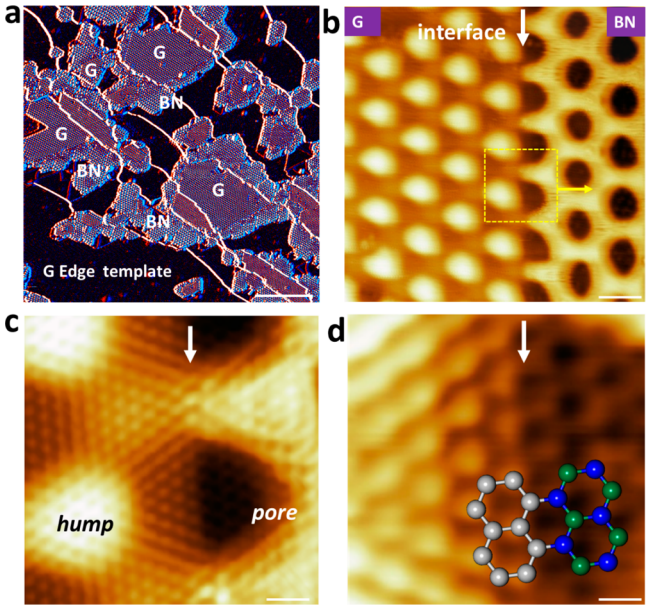

Figure 1. STM imaging of atomically sharp G/BN heterointerface. (a) Following borazine dose (5 L) at 800 K, BN domains nucleate on the edges of graphene on Ru(0001). (b) A sharp G/BN interface with length <21 nm at 800 K. (c) Magnified view of panel b showing the formation of a seamless G/BN interface at the atomic scale. (d) Magnified view of panel c showing a zigzag edge of graphene bonded to a zigzag edge of BN at the interface. Scale bars in a−d are 50, 2.5, 0.5, and 0.25 nm, respectively.

moiré structures occurring close to the G/BN interfaces. The formation of irregularity away from the interface is due to the merging of polycrystalline BN domains, as shown in STM images of Figure 2a,e and Supporting Information Figure S3. The formation of discontinuities at the interface is attributed to the unrelaxed interface strain (Figure 2b,c,h). One way to relieve the interfacial strain is the formation of heart-shaped moiré structures at the G/BN interface, which can be considered as a type of misfit dislocation in two-dimensional crystals as discussed below.

Owing to a lattice mismatch of ∼1.8% between graphene and boron nitride,[33] strain-induced discontinuities are expected to occur at the G/BN interface. Consistent with this, we frequently observed the "breakage" of Moiré pattern at the G/BN boundaries (as marked by yellow arrows in Figure 2b,c and Supporting Information Figure S1) when the interface length exceeds ∼20 nm. The discontinuity at the G/BN interface arises from (i) strain-induced formation of multivacancies as revealed in the close-up STM images of Supporting Information Figure S 1f,g, and (ii) distortion of the BN lattice at the interface where different BN domains merge (Figure 2h). However, we found that in cases where interface continuity is maintained, it is invariably accompanied by the presence of heart-shaped Moiré structures that are formed close to the G/BN interface (Figure 2d,f,g and Supporting Information Figure S2). In most cases, discontinuities and misfit dislocations are mutually exclusive, especially in single BN domain that nucleates on the same graphene edge. Two regions "A" and "B" are highlighted in Figure 2h; only discontinuities are observed in the BN attached to graphene's edge "A". In contrast, heart-shaped dislocations are found in BN attached to edge "B", whereby its regular moiré pattern can be preserved. These observations indicate that the introduction of

dx.doi.org/10.1021/nl501900x | Nano Lett. 2014, 14, 5133−5139

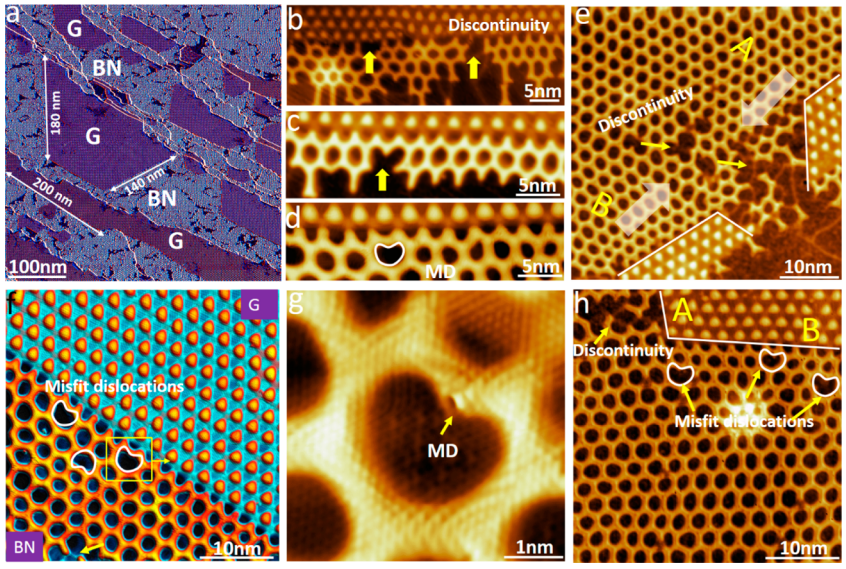

Figure 2. Formation of MD at extended G/BN interface (>100 nm). (a) Large-scale STM image of coexisting G/BN domains with extended linear sharp interface; grown at 800 K with an increased ratio of $\mu_C/\mu_{B/N}$ (in the range between 0.4 and 0.6); the growth of G islands (~0.5 monolayer) followed by a dosage of borazine (30 Langmuirs) to cover all the remaining Ru surface. (b,c) Interface discontinuity (as marked in yellow arrows) occurs when the length of 1D interface extends above ~20 nm. (d) MD sets in to relieve interface strain and keep the continuity of G/BN boundary. (e) The discontinuities in BN moiré pattern appear in the regions where different BN domains merge. (f) Magnified view shows the formation of MD in BN Moiré pattern near the interface zones [note: the moiré irregularity appearing at the bottom of this image (as marked in yellow arrow) is due to the merging of multiple BN domains]. (g) High-resolution imaging of MD reveals the structure of the dislocation core. (h) Misfit dislocations in BN appears close to graphene's A edge, while discontinuities in BN appear close to graphene's B edge.

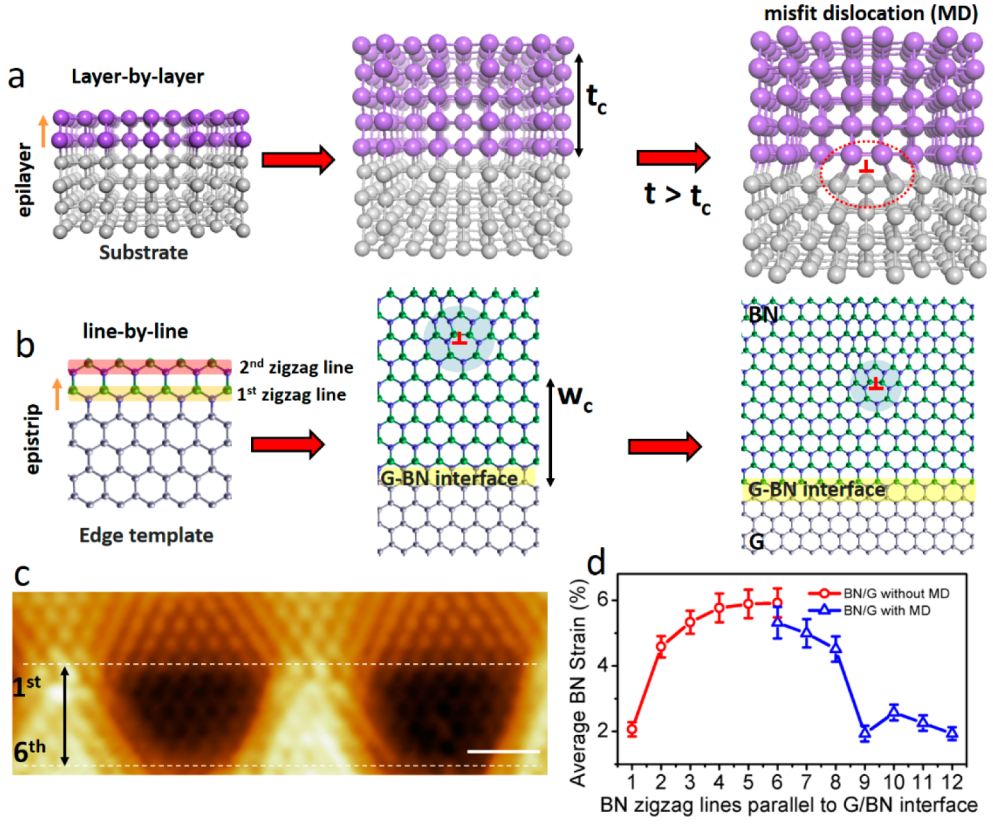

Figure 3. (a) The formation of misfit dislocations in layered heteroepitaxial growth of thin film above a critical thickness (t_c). (b) For the graphene edge-templated heterogrowth of BN, a misfit dislocation forms above the critical width (w_c) to relieve strain. (c) Atomic-resolved coherent lattice at the G/BN interface for strain analysis: BN zigzag line right at the interface is numbered as first line. (d) Strain propagation parallel to the interface before and after introducing MD. Error bar represents the standard deviation of the measurement of averaged strain of BN zigzag lines in three different regions with (blue) and without (red) misfit dislocations.

dx.doi.org/10.1021/nl501900x | *Nano Lett.* 2014, 14, 5133−5139

dislocations helps to release the interface strain so that regular BN moiré pattern can be maintained.

We also found that the majority of such distorted, "heart-shaped" Moiré structures (as opposed to the regular round moiré structures) are distributed along the interface and spaced out irregularly by several Moiré units (Figure 2f and Supporting Information Figure S2). The majority of the heart-shaped moiré structures occur in the first row of BN moiré pattern (counted from the interface) and few appear in the second row (Figure 2f,h and Supporting Information Figure S2). The "heart-shaped" Moiré structure will also be introduced where two nanomesh "pores" overlap and intersect at an angle of 60° (indicated in Supporting Information Figure S4 and S5). Each "heart-shaped" Moiré structure consists of 20−30 zigzag BN lines. In line with recent theoretical predictions, this irregularity is presumably due to the formation of edge dislocations, which were proposed to consist of pentagon−heptagon pairs.[7,34−36] Such a heptagon−pentagon dislocation (as shown in Figure 3b) can be viewed as a result of inserting a semi-infinite strip of atoms along the armchair high-symmetry direction in h-BN lattice with its Burgers vector oriented along the zigzag direction.[34]

To examine the strain profile around the dislocation, we extracted the strain profile at the interface from the atomically resolved STM imaged bonds. It is challenging to determine the actual lattice constant in this system using STM imaging because substrate interaction,[37,38] electron localizations,[39] and elastic response[40] during scanning are reported to have a significant influence on the apparent corrugation of adatoms in Moiré patterns. However, the applied tunneling conditions are expected to have negligible influence on the lateral distance between adjacent imaged spots. We also found that as-measured lateral expansion in the lattice constant is the major contribution to the interfacial strain compared to the small vertical corrugation of adjacent lattice spots in graphene and BN. Hence, we consider the average strain of each BN or graphene zigzag line by measuring the ratio between a specified length and the total number of lattice space within in order to minimize errors in determining each lattice space individually (see Supporting Information Figure S6 for the detailed procedures of strain calculation). The strain profile reveals that the graphene lattice is not perturbed during the growth of BN, and strain propagates mainly in the BN side of the interface. Another observation is that misfit dislocations in the BN Moiré superstructure, which are made of nonhexagonal rings, often appear at ∼5 lattice constants away from the interface. To understand how the strain propagates with the width of the BN strip, we extract a width-dependent average strain of each BN zigzag line parallel to the G/BN interface (starting from the interface: first line to sixth line as indicated in Figure 3c). As shown in Figure 3d, which describes the strain profile along the perpendicular direction from the interface, the strain in BN rapidly builds up in the first three atomic rows and reaches a maximum value of 5.9% at the sixth row. Since the lattice constant of BN (epistrip) is larger than that of graphene (edge substrate), the BN lattice is compressed at the interface. The first BN atomic zigzag line at the interface experiences the uniaxial compression force from the graphene lattice, which reduces the lattice constant of h-BN and generates a positive strain value of ∼1.9%. It must be pointed out that the average strain of pristine h-BN on Ru is slightly larger (positive 2.2%). The interface strain builds up from the interface and eventually reaches the maximum value (as measured from the experimental data) at a critical width of 5−6 atomic BN zigzag lines (equal to $\sim 5-6[\sqrt{3}a/)2] = 1.08-1.29$ nm, a is the lattice constant of BN). The occurrence of maximum strain agrees with the location where the misfit dislocations are usually found, which is typically at a distance of 1.08 nm from the interface (Figure 2g and Supporting Information Figure S2). As reflected in the strain profile analysis, the strain is relieved at regions where misfit dislocations occur, the strain decays within the first three rows (from the misfit dislocations (MD) position), and returns to its bulk value (i.e., the strain in the BN nanomesh) at the fourth row (Figure 3d).

We have carried out ab initio calculations of strain profiles of free-standing G/BN heterointerfaces with and without the dislocations (see Supporting Information for the details). We have performed careful convergence tests of all our results with respect to the numerical parameters of the methodology employed. Structural optimization has been performed with residual forces of <0.005 eV/Å on each atom. Our calculations are performed with graphene/BN ribbons that are periodic (infinite) along the directions of the interface and finite in the perpendicular direction. We consider the misfit dislocations present in two types of G/BN boundaries: C−N and C−B bonded interfaces because these boundary types cannot be discriminated in our STM imaging. Our calculation results show that the average strain decreases around the adjacent BN zigzag lines when a dislocation is included in the zigzag line at a distance of ∼1.08 nm away from interface (Supporting Information Figure S7). Hence both the experimental observation and theoretical results support that the "remote" placement of dislocation away from the interface serves the function of relieving the strain at the interface.

As mentioned above, the strain at the G/BN heterointerfaces is certainly modulated by the underlying metal surface. To eliminate the influence of the metal, the hybrid film was delaminated using O_2 intercalation. The hybrid film was successfully decoupled after annealing the film at 400 K at a low partial pressure ($\sim 2 \times 10^{-8}$ mbar) of oxygen gas (Figure 4a−c) for 10−15 min, as can be judged from the remarkably reduced corrugation in G and BN (inset of Figure 4b). Similar recipes for the decoupling of graphene on metal surface had been reported in previous work.[41−45] The maximum strain of BN at decoupled boundaries is slightly reduced (from 5.9 to 4.0%) due to the exclusion of strong substrate interactions but the strain accumulates as we move away from the interface (Supporting Information Figure S8). We can conclude that although the metal substrate introduces additional strain at the G/BN interface, it does not change the general trend of strain dependence with the distance from the interface.

One interesting difference here between defect propagation in 2D and 3D heteroepitaxy is that in the former case the misfit dislocation is located ∼1.08 nm away from the interface, whereas it is known that in 3D heteroepitaxy growth a network of the dislocations will be formed at the interface either by the nucleation at the interface or migration into the interface.[24] In contrast, the defects are trapped in the case of 2D BN heteroepitaxy due to strong interaction with the Ru substrate.

Zigzag type G/BN heterointerface has been predicted to possess interesting properties such as half-metallicity, anti-ferromagnetism, and other transport properties.[9,13,18,46,47] The ability to resolve the zigzag type coherent G/BN interface allows us to investigate its local electronic states using scanning tunneling spectroscopy (STS). For freestanding graphene, localized states at the zigzag edges produce flat bands and sharp

dx.doi.org/10.1021/nl501900x | Nano Lett. 2014, 14, 5133−5139

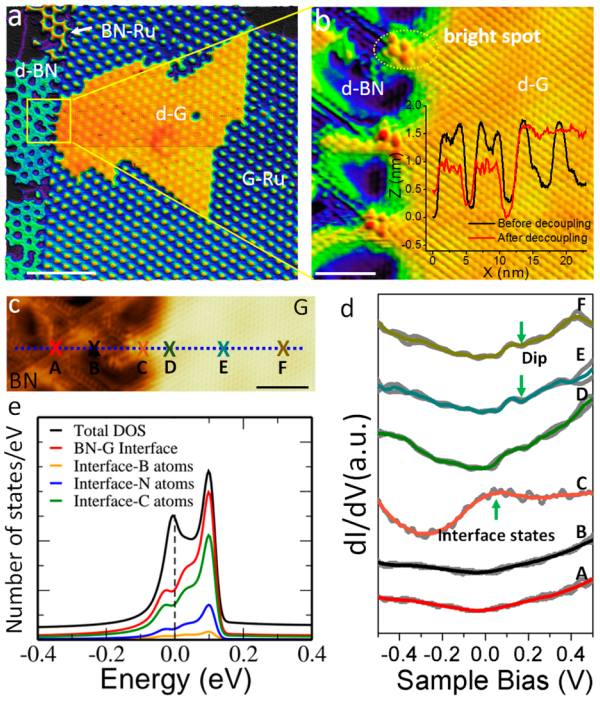

Figure 4. Probing the intrinsic electronic states at the G/BN interface after O_2 intercalation. (a) Large-scale STM image to show the coexistence of decoupled G/BN interface and coupled interface. (b) The presence of interface states generates bright spots at the interface of G/BN after decoupling. Inset: height profile along the direction perpendicular to the interface of G/BN, before and after decoupling. (c) STM imaging of decoupled graphene/BN interface. (d) STS spectra collected along the line perpendicular to the G/BN interface as marked in c. (e) Simulation of total density of states of G/BN hybrid ribbons and the projected density of states at G/BN interfaces. Scale bars in a–c are 20, 2, and 2.5 nm, respectively.

density of states (DOS) at the Fermi Level (E_F).[48,49] However, such zigzag states are quenched when graphene is attached to Ru, because the orbital hybridization between carbon and Ru depletes the DOS near E_F. Upon the bonding of graphene edge to BN, such localized edge states remain absent due to the coupling with metal, as evident from the STS study. In contrast, a great enhancement of the differential conductance (dI/dV) is observed at the decoupled G/BN interface (Figure 4d), which results in the appearance of distinct bright spots (due to enhanced local DOS) when imaged by STM (Figure 4b, c). Such bright spots are absent in as-grown G/BN interfaces (Figures 1 and 2). The STS collected at the decoupled BN sites (points A and B marked in Figure 4c) is relatively featureless with a low tunneling conductance owing to its insulating nature, while the decoupled graphene close to the interface displays p-doping as reflected by the presence of a dip at ~0.15 eV (Dirac point) in the STS curve (collected at E and F points in Figure 4d).[50] The differential conductance around E_F slightly increases as the tip moves close to the G/BN interface (point D). In contrast, a broad feature that peaked around 80 meV appears in the dI/dV spectrum taken at the "bright" spots right at the G/BN interface (point C in Figure 4d), which can be explained by the enhancement of LDOS around E_F from the strong mixing of π-orbitals between C and N (B) at the interface (Figure 4d).[51]

To understand the interface states observed in dI/dV spectra, we carried out ab initio calculations of the electronic structures of G/BN coherent interface with a periodic array (17.5 Å) of 5–7 dislocation cores located at a distance of 1.15 nm away from the interface. We employ the same methodology as in the strain-profile calculations. Our ab initio calculations confirm the experimentally probed electronic properties of the G/BN interfaces. The total DOS of the G/BN interface is shown in Figure 4e and the degree of localization of these electronic states at the interface can be analyzed by its partial DOS (PDOS). The total DOS (the black curve in Figure 4e) shows two sharp peaks around E_F. The first one, right at E_F, is only partially localized on the interface atoms with ~40% of the total DOS deriving from these atoms. A different scenario is observed for the second peak, located at ~0.1 eV above E_F; the PDOS curves show that this peak is associated with states that are strongly localized at the interface with ~90% contribution from the orbitals of the interface atoms. These results are consistent with the experimental measurements. For example, the experimentally observed broad peak with width of ~0.4 eV probably originate from the overlap of the two peaks predicted in the DFT calculations.

Summary. In summary, our results demonstrate that atomically abrupt G/BN heterointerfaces can be grown by nucleating BN at the edges of existing graphene islands at 800 K. Long and sharp G/BN interface can be formed by relieving the accumulated strain through the formation of misfit dislocations situated at ~1 nm from the interface. The migration of dislocations to the interface of G/BN is hindered owing to a high-diffusion-energy barrier on metal, which offers a unique strategy to generate atomically sharp two-dimensional heterointerface. In the absence of misfit dislocation, the interface becomes discontinuous at length scale of tens of nanometers. The electronic states associated with the formation of the coherent G/BN boundaries are characterized by a strong 1D confinement along the boundary, leading to the enhancement of the density of states near the Fermi level.

Experimental Section. Sample preparation and STM characterization: The experiments were performed in an ultrahigh-vacuum chamber equipped with a STM and an adjoined sample preparation chamber with a base pressure of 1.5×10^{-10} mbar. The clean Ru(0001) was exposed to a gas flux of C_2H_4 gas (National Oxygen Pte Ltd., purity 99.99%) at a partial pressure of 5×10^{-8} mbar for 2–10 min with the substrate heated up to ~900–1000 K to grow submonolayer graphene (~0.3–0.8 ML). To synthesize G/BN heterostructures with sharp interfaces, as-prepared graphene/Ru(0001) was annealed in vaporized borazine with a partial pressure of $\sim 1 \times 10^{-8}$ mbar at 800 K for 5 min. After growth, the sample was characterized by a SPECS STM 150 Aarhus unit with the Nanonis (SPECS) SPM control system at 298 K.

Ab Initio Calculations. We employ a first-principles approach based on Kohn–Sham density functional theory (KS-DFT),[52] as implemented in the SIESTA code.[53] The generalized gradient approximation is used for the exchange-correlation term.[54] Interactions between valence electrons and ionic cores are described by Troullier–Martins pseudopotentials.[55] A double-ζ pseudoatomic basis set augmented with polarization orbitals is employed with an energy cutoff of 0.01 Ry.

■ ASSOCIATED CONTENT

Supporting Information

Additional information and figures. This material is available free of charge via the Internet at http://pubs.acs.org.

dx.doi.org/10.1021/nl501900x | Nano Lett. 2014, 14, 5133–5139

AUTHOR INFORMATION

Corresponding Author

*E-mail: chmlohkp@nus.edu.sg.

Author Contributions

#J.L. and L.C.G. contributed equally.

Notes

The authors declare no competing financial interest.

ACKNOWLEDGMENTS

K.P.L. thanks funding support from MOE Tier 2 "From in-situ observation to the growth scaling of graphene quantum dots" R-143-000-493-112. A.H.C.N. acknowledges the NRF-CRP award "Novel 2D materials with tailored properties: beyond graphene" (R-144-000-295-281). L.C.G. and R.W.N. acknowledge funding from the Brazilian agencies CNPq, FAPEMIG, and INCT de Nanomateriais de Carbono.

REFERENCES

(1) Hull, R.; Bean, J. C. *J. Vac. Sci. Technol. A* **1989**, *7*, 2580−2585.
(2) Jain, S. C.; Harker, A. H.; Cowley, R. A. *Philos. Mag. A* **1997**, *75*, 1461−1515.
(3) Bernardi, M.; Palummo, M.; Grossman, J. C. *Phys. Rev. Lett.* **2012**, *108*, 226805.
(4) Ci, L.; Song, L.; Jin, C. H.; Jariwala, D.; Wu, D. X.; Li, Y. J.; Srivastava, A.; Wang, Z. F.; Storr, K.; Balicas, L.; Liu, F.; Ajayan, P. M. *Nat. Mater.* **2010**, *9*, 430−435.
(5) Liu, L.; Park, J.; Siegel, D. A.; McCarty, K. F.; Clark, K. W.; Deng, W.; Basile, L.; Idrobo, J. C.; Li, A. P.; Gu, G. *Science* **2014**, *343*, 163−167.
(6) Liu, Z.; Ma, L. L.; Shi, G.; Zhou, W.; Gong, Y. J.; Lei, S. D.; Yang, X. B.; Zhang, J. N.; Yu, J. J.; Hackenberg, K. P.; Babakhani, A.; Idrobo, J. C.; Vajtai, R.; Lou, J.; Ajayan, P. M. *Nat. Nanotechnol.* **2013**, *8*, 119−124.
(7) Levendorf, M. P.; Kim, C. J.; Brown, L.; Huang, P. Y.; Havener, R. W.; Muller, D. A.; Park, J. *Nature* **2012**, *488*, 627−632.
(8) Lu, J.; Zhang, K.; Liu, X. F.; Zhang, H.; Sum, T. C.; Neto, A. H. C.; Loh, K. P. *Nat. Commun.* **2013**, *4*, 2681.
(9) Jung, J.; Qiao, Z. H.; Niu, Q.; MacDonald, A. H. *Nano Lett.* **2012**, *12*, 2936−2940.
(10) Kim, S. M.; Hsu, A.; Araujo, P. T.; Lee, Y. H.; Palacios, T.; Dresselhaus, M.; Idrobo, J. C.; Kim, K. K.; Kong, J. *Nano Lett.* **2013**, *13*, 933−941.
(11) Chang, C. K.; Kataria, S.; Kuo, C. C.; Ganguly, A.; Wang, B. Y.; Hwang, J. Y.; Huang, K. J.; Yang, W. H.; Wang, S. B.; Chuang, C. H.; Chen, M.; Huang, C. I.; Pong, W. F.; Song, K. J.; Chang, S. J.; Guo, J. H.; Tai, Y.; Tsujimoto, M.; Isoda, S.; Chen, C. W.; Chen, L. C.; Chen, K. H. *ACS Nano* **2013**, *7*, 1333−1341.
(12) Liu, Y. Y.; Bhowmick, S.; Yakobson, B. I. *Nano Lett.* **2011**, *11*, 3113−3116.
(13) Ramasubramaniam, A.; Naveh, D. *Phys. Rev. B* **2011**, *84*, 075405.
(14) Jiang, J. W.; Wang, J. S.; Wang, B. S. *Appl. Phys. Lett.* **2011**, *99*, 043109.
(15) Kinaci, A.; Haskins, J. B.; Sevik, C.; Cagin, T. *Phys. Rev. B* **2012**, *86*, 115410.
(16) Zhou, Y. G.; Wang, Z. G.; Yang, P.; Gao, F. *J. Phys. Chem. C* **2012**, *116*, 7581−7586.
(17) Gao, Y. B.; Zhang, Y. F.; Chen, P. C.; Li, Y. C.; Liu, M. X.; Gao, T.; Ma, D. L.; Chen, Y. B.; Cheng, Z. H.; Qju, X. H.; Duan, W. H.; Liu, Z. F. *Nano Lett.* **2013**, *13*, 3439−3443.
(18) Yu, Z. Z.; Hu, M. L.; Zhang, C. X.; He, C. Y.; Sun, L. Z.; Zhong, J. X. *J. Phys. Chem. C* **2011**, *115*, 10836.
(19) Sutter, P.; Cortes, R.; Lahiri, J.; Sutter, E. *Nano Lett.* **2012**, *12*, 4869−4874.
(20) Zhao, S. J.; Xue, J. M. *J. Phys. D: Appl. Phys.* **2013**, *46*, 135303.
(21) Han, G. H.; Rodriguez-Manzo, J. A.; Lee, C. W.; Kybert, N. J.; Lerner, M. B.; Qi, Z. J.; Dattoli, E. N.; Rappe, A. M.; Drndic, M.; Johnson, A. T. C. *ACS Nano* **2013**, *7*, 10129.
(22) Fitzgerald, E. A. *Mater. Sci. Rep.* **1991**, *7*, 91−142.
(23) Harrison, W. A.; Kraut, E. A.; Waldrop, J. R.; Grant, R. W. *Phys. Rev. B* **1978**, *18*, 4402−4410.
(24) Jesser, W. A.; Kui, J. M. *Mater. Sci. Eng., A* **1993**, *164*, 101.
(25) Marchini, S.; Gunther, S.; Wintterlin, J. *Phys. Rev. B* **2007**, *76*, 075429.
(26) Goriachko, A.; He, Y. B.; Knapp, M.; Over, H.; Corso, M.; Brugger, T.; Berner, S.; Osterwalder, J.; Greber, T. *Langmuir* **2007**, *23*, 2928.
(27) Lu, J.; Yeo, P. S. E.; Zheng, Y.; Xu, H.; Gan, C. K.; Sullivan, M. B.; Neto, A. H. C.; Loh, K. P. *J. Am. Chem. Soc.* **2013**, *135*, 2368.
(28) de Parga, A. L. V.; Calleja, F.; Borca, B.; Passeggi, M. C. G.; Hinarejos, J. J.; Guinea, F.; Miranda, R. *Phys. Rev. Lett.* **2008**, *100*, 056807.
(29) Bhaviripudi, S.; Jia, X.; Dresselhaus, M. S.; Kong, J. *Nano Lett.* **2010**, *10*, 4128−4133.
(30) Li, X.; Magnuson, C. W.; Venugopal, A.; An, J.; Suk, J. W.; Han, B.; Borysiak, M.; Cai, W.; Velamakanni, A.; Zhu, Y.; Fu, L.; Vogel, E. M.; Voelkl, E.; Colombo, L.; Ruoff, R. S. *Nano Lett.* **2010**, *10*, 4328−4334.
(31) Vlassiouk, I.; Smirnov, S.; Regmi, M.; Surwade, S. P.; Srivastava, N.; Feenstra, R.; Eres, G.; Parish, C.; Lavrik, N.; Datskos, P.; Dai, S.; Fulvio, P. *J. Phys. Chem. C* **2013**, *117*, 18919−18926.
(32) Yan, Z.; Peng, Z.; Tour, J. M. *Acc. Chem. Res.* **2014**, *47*, 1327.
(33) Xue, J. M.; Sanchez-Yamagishi, J.; Bulmash, D.; Jacquod, P.; Deshpande, A.; Watanabe, K.; Taniguchi, T.; Jarillo-Herrero, P.; Leroy, B. J. *Nat. Mater.* **2011**, *10*, 282.
(34) Yazyev, O. V.; Louie, S. G. *Phys. Rev. B* **2010**, *81*, 195420.
(35) Liu, Y. Y.; Zou, X. L.; Yakobson, B. I. *ACS Nano* **2012**, *6*, 7053.
(36) Gibb, A. L.; Alem, N.; Chen, J. H.; Erickson, K. J.; Ciston, J.; Gautam, A.; Linck, M.; Zettl, A. *J. Am. Chem. Soc.* **2013**, *135*, 6758.
(37) Gyamfi, M.; Eelbo, T.; Wasniowska, M.; Wiesendanger, R. *Phys. Rev. B* **2011**, *83*, 153418.
(38) Wang, B.; Bocquet, M. L.; Marchini, S.; Gunther, S.; Wintterlin, J. *Phys. Chem. Chem. Phys.* **2008**, *10*, 3530.
(39) Stradi, D.; Barja, S.; Diaz, C.; Garnica, M.; Borca, B.; Hinarejos, J. J.; Sanchez-Portal, D.; Alcami, M.; Arnau, A.; de Parga, A. L. V.; Miranda, R.; Martin, F. *Phys. Rev. B* **2012**, *85*, 121404(R).
(40) Koch, S.; Stradi, D.; Gnecco, E.; Barja, S.; Kawai, S.; Diaz, C.; Alcami, M.; Martin, F.; de Parga, A. L. V.; Miranda, R.; Glatzel, T.; Meyer, E. *ACS Nano* **2013**, *7*, 2927.
(41) Sutter, P.; Sadowski, J. T.; Sutter, E. A. *J. Am. Chem. Soc.* **2010**, *132*, 8175.
(42) Grånäs, E.; Knudsen, J.; Schröder, U. A.; Gerber, T.; Busse, C.; Arman, M. A.; Schulte, K.; Andersen, J. N.; Michely, T. *ACS Nano* **2012**, *6*, 9951−9963.
(43) Larciprete, R.; Ulstrup, S.; Lacovig, P.; Dalmiglio, M.; Bianchi, M.; Mazzola, F.; Hornekær, L.; Orlando, F.; Baraldi, A.; Hofmann, P.; Lizzit, S. *ACS Nano* **2012**, *6*, 9551−9558.
(44) Jin, L.; Fu, Q.; Zhang, H.; Mu, R.; Zhang, Y.; Tan, D.; Bao, X. *J. Phys. Chem. C* **2012**, *116*, 2988−2993.
(45) Lu, J.; Castro Neto, A. H.; Loh, K. P. *Nat. Commun.* **2012**, *3*, 823.
(46) Kan, E. J.; Wu, X. J.; Li, Z. Y.; Zeng, X. C.; Yang, J. L.; Hou, J. G. *J. Chem. Phys.* **2008**, *129*, 084712.
(47) Liu, Z. M.; Zhu, Y.; Yang, Z. Q. *J. Chem. Phys.* **2011**, *134*, 074708.
(48) Nakada, K.; Fujita, M.; Dresselhaus, G.; Dresselhaus, M. S. *Phys. Rev. B* **1996**, *54*, 17954.
(49) Tao, C. G.; Jiao, L. Y.; Yazyev, O. V.; Chen, Y. C.; Feng, J. J.; Zhang, X. W.; Capaz, R. B.; Tour, J. M.; Zettl, A.; Louie, S. G.; Dai, H. J.; Crommie, M. F. *Nat. Phys.* **2011**, *7*, 616.
(50) Zhang, Y. B.; Brar, V. W.; Wang, F.; Girit, C.; Yayon, Y.; Panlasigui, M.; Zettl, A.; Crommie, M. F. *Nat. Phys.* **2008**, *4*, 627.
(51) Li, Y.; Mazzarello, R. *Phys. Rev. B* **2013**, *88*, 045317.
(52) Kohn, W.; Sham, L. J. *Phys. Rev.* **1965**, *140*, 1133.

(53) Soler, J. M.; Artacho, E.; Gale, J. D.; Garcia, A.; Junquera, J.; Ordejon, P.; Sanchez-Portal, D. *J. Phys.: Condens Mater.* **2002**, *14*, 2745.
(54) Perdew, J. P.; Burke, K.; Ernzerhof, M. *Phys. Rev. Lett.* **1996**, *77*, 3865.
(55) Troullier, N.; Martins, J. L. *Phys. Rev. B* **1991**, *43*, 1993.

dx.doi.org/10.1021/nl501900x | *Nano Lett.* 2014, 14, 5133−5139